Journal of ELECTRONIC MATERIALS, Vol. 47, No. 10, 2018
https://doi.org/10.1007/s11664-018-6499-8

Facile Preparation of Hybrid Films Based on MnO_2 and Reduced Graphene Oxide for a Flexible Supercapacitor

SHIQING SUN,[1,2,3] GUOHUA JIANG ,[1,2,3,4,5] YONGKUN LIU,[1,2,3] BO YU,[1,2,3] and UWAMAHORO EVARISTE[1,2,3]

1.—Department of Polymer Materials, Zhejiang Sci-Tech University, Hangzhou 310018, China. 2.—National Engineering Laboratory for Textile Fiber Materials and Processing Technology (Zhejiang), Hangzhou 310018, China. 3.—Key Laboratory of Advanced Textile Materials and Manufacturing Technology (ATMT), Ministry of Education, Hangzhou 310018, China. 4.—Institute of Smart Fiber Materials, Zhejiang Sci-Tech University, Hangzhou 310018, China. 5.—e-mail: ghjiang_cn@zstu.edu.cn

Supercapacitors (SCs) have drawn considerable attention as one of the energy storage devices. The key to fabricating flexible supercapacitors lies in the acquirement of flexible electrodes. In this study, the manganese oxide (MnO_2) and reduced graphene oxide (RGO) hybrid films (MnO_2/RGO) were prepared by a filtration deposition and thermal reduction technique. Electrochemical measurements show that the hybrid films exhibit a specific capacitance of 333.9 F g^{-1} at 0.5 A g^{-1}, and 87% capacitance after 3000 cycles at 0.5 A g^{-1}. The flexible symmetric SCs was further fabricated with two pieces of MnO_2/RGO hybrid films as electrodes. The fabricated flexible and sandwich type symmetrical SCs exhibited a safe working range with a potential window of 0–0.7 V with a maximum energy density of 23.5 Wh kg^{-1} at 0.5 A g^{-1} and the maximum power density of 1716.9 W kg^{-1} at 2.25 A g^{-1}.

Key words: Electronic material, composite films, energy storage, supercapacitor

INTRODUCTION

Supercapacitors (SCs) have drawn considerable attention as one of the energy storage devices because of their high-energy density and power density, fast charge–discharge rates and excellent cyclic life.[1–5] Especially, the flexible solid-state SCs have gained intense research focus because of their fast charge–discharge rate, light weight, ease of handling, long cycle life, outstanding safety and environmental friendliness.[6–8] The typical two-dimensional (2-D) graphene nanomaterials have been extensively studied as flexible electrode materials, due to their fascinating physical and chemical properties, high flexibility and excellent mechanical strength.[9] However, graphene by itself can be utilized as a SCs electrode with extraordinary cyclic stability but the magnitude of specific capacitance is low compared to other conducting polymer or metal oxide based supercapacitors.[10–13] Moreover, the performance of pristine graphene sheets as SCs electrode materials is further limited due to aggregation and restacking caused by van der Waals interactions between the adjacent layers leading to reduction in effective surface area.[14] The decrease in surface area is the main reason behind the restriction of carbon materials in high energy storage devices as the electrolyte cannot perforate into the planes of the material thereby decreasing the electrical double layer formed at the interface.[2] To overcome this challenge, one approach to improve the surface area of graphene materials is combining them with nanostructured metal oxides.[15–19] Manganese oxide (MnO_2) has advantages in environmental friendless, low cost and high theoretical specific capacitance. Their electrochemical performance can be improved by engineering of MnO_2 into composites or specific nanos-

(Received April 9, 2018; accepted June 29, 2018; published online July 9, 2018)

tructures.[20–23] Here, a simple and facile approach has been presented to prepare MnO_2/RGO hybrid films by a filtration deposition technique. The obtained hybrid films were further used as electrode materials for fabrication of flexible and sandwich type solid-state-symmetrical SCs.

EXPERIMENTAL PROCEDURE

Materials

Manganese sulfate ($MnSO_4{\cdot}H_2O$), and p-phenylenediamine (PPD) were purchased from Aladdin Co. Ltd. (China). Sodium sulfate anhydrous ($NaSO_4$) was obtained from Macklin Biochemical Co. Ltd. (Shanghai). Potassium permanganate ($KMnO_4$), potassium persulfate ($K_2S_2O_8$), phosphorus pentoxide (P_2O_5), 30% hydrogen peroxide (H_2O_2), concentrated sulfuric acid (H_2SO_4,98%) and nitric acid (HNO_3, 98%) were purchased from Hangzhou Sanying Chemical Co. Ltd.

Preparation of Electrode Materials and Assembled Supercapacitors

The MnO_2 microspheres (MnO_2 MPs) were synthesized via a reduction route.[24] Graphene oxide (GO) was prepared by oxidation of graphite using a modified Hummers method.[25] The MnO_2 MPs were further mixed with GO (4 mg mL^{-1}) and PPD (10 mg mL^{-1}) suspension at different mass ratios. The obtained mixture was added into a filtration unit covering a cellulose membrane without stirring. The solvent was evaporated slowly until dry to form hybrid MnO_2/GO film. The hybrid MnO_2/GO film was further heated in the tube furnace in nitrogen condition at 400°C for 3 h (2°C min^{-1}) to remove excess reagent and reduce GO to form MnO_2/RGO hybrid films. The flexible symmetric SCs was fabricated with two pieces of MnO_2/RGO hybrid films as electrodes. Two film electrodes were separated by electrolyte (1.0 M Na_2SO_4) soaked separator (NKK Co. Ltd., 100 μm), and attached to a conductive copper foil for external circuit connection.

Characterization

The microstructures, crystal phases and morphologies of as-obtained product was analyzed by field emission scanning electron microscopy (FE-SEM; ULTRA-55), x-ray photoelectron spectroscopy (XPS; ESCALab220i-XL), transmission electron microscopy (TEM; JSM-2100) and x-ray diffractometer (XRD; Siemens Diffractometer D5000).

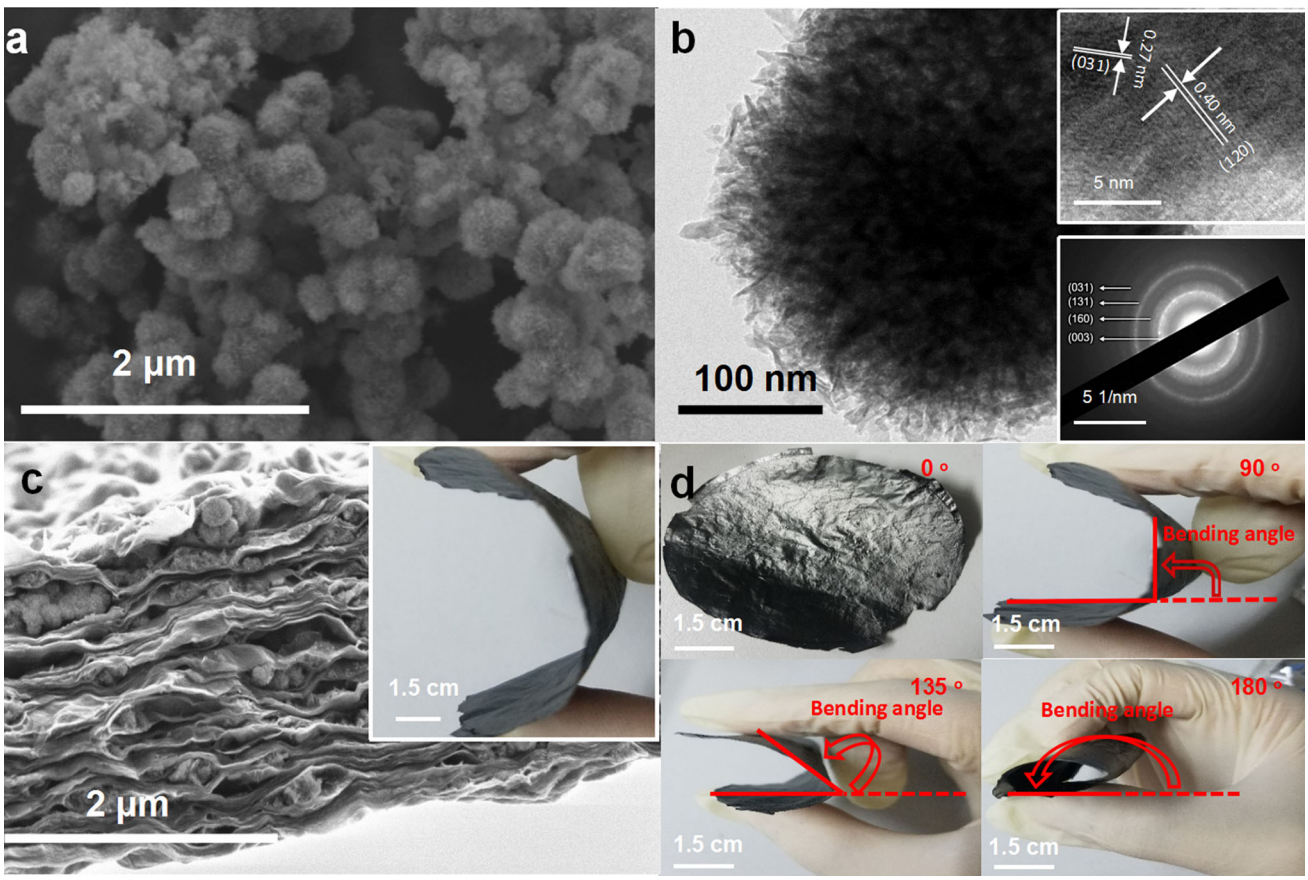

Fig. 1. (a) SEM image of MnO_2 MPs. (b) TEM, HRTEM images and SAED pattern of MnO_2 MPs. (c) SEM image and digital picture (inset) of MnO_2/RGO hybrid films. (d) The MnO_2/RGO hybrid films at different folding angle.

The electrochemical characteristics and the cycling stability of the prepared electrode was tested by a CHI660e (Shanghai) electrochemical work station and a LAND battery system, respectively.

The electrochemical characteristics of the MnO_2/RGO hybrid films and fabricated SCs was tested in the three-electrode electrochemical measurements, containing electrolyte with 1.0 M $NaSO_4$ aqueous

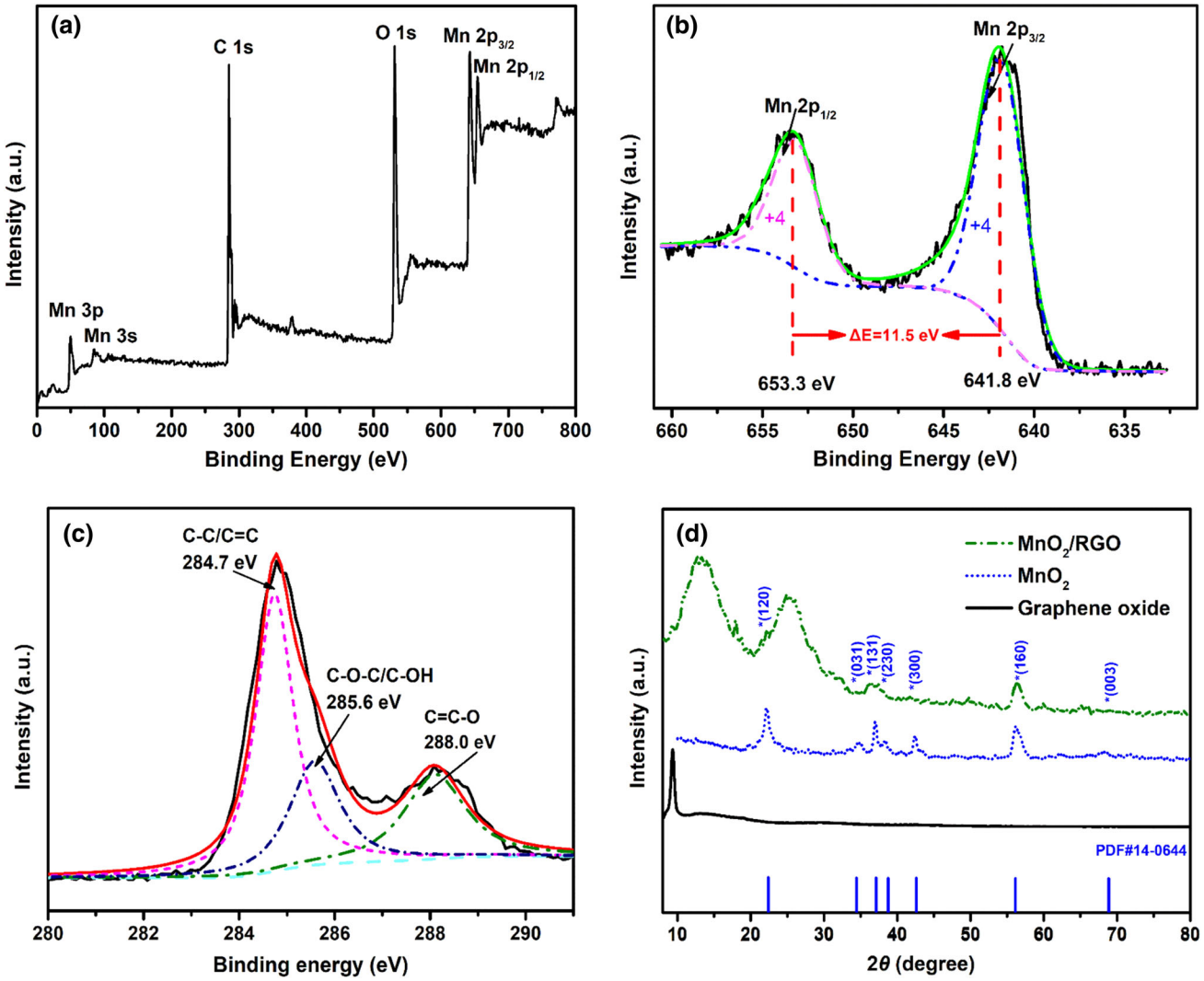

Fig. 2. (a) XPS survey of MnO_2 MPs. High resolution of (b) Mn 2*p* and (c) C 1s. (d) XRD patterns of GO, MnO_2 MPs and MnO_2/RGO hybrid films.

Table I. The electronic performance of hybrid films with various mass ratios

GO: MnO_2 (wt.%)	Internal resistance (Ω)	Specific capacitance (F g^{-1})
10:0	4.88 ± 0.02	17.2 ± 0.1
10:1	5.77 ± 0.03	74.9 ± 0.3
10:2	5.59 ± 0.03	93.8 ± 0.4
10:4	5.64 ± 0.04	175.0 ± 0.9
10:6	6.01 ± 0.03	333.9 ± 1.1
10:8	5.94 ± 0.04	195.9 ± 1.0
10:10	6.75 ± 0.05	315.4 ± 1.3

All the data in Table I have been measured three times for average value.

solution, the working electrode with hybrid film (1×1 cm^2) and the reference electrodes with a Hg/HgO electrode. The cyclic voltammetry (CV), galvanostatic charge–discharge (GCD) tests and electrochemical impedance spectroscopy (EIS) were all measured in a 1.0 M $NaSO_4$ aqueous electrolyte. Furthermore, EIS was also measured by a small amplitude of 5 mV at a range of frequencies from 100 kHz to 0.01 Hz. The cyclic stability of fabricated SCs was measured via repeated charge–discharge processes at the potential window of 0–0.7 V within 1.0 M $NaSO_4$ aqueous electrolyte. The specific capacity (C), specific energy (E) and specific power (P) of the SCs can be calculated by the charge–discharge curves on the basis of the equations:

$$C = (I \times \Delta t)/(m \times \Delta V), \quad (1)$$

$$E = \left(C \times \Delta V^2\right)/2, \quad (2)$$

$$P = E/\Delta t. \quad (3)$$

Here, I is the discharge current, Δt is the discharge time, m is the mass of the active material, and ΔV is the width of the potential window.

RESULTS AND DISCUSSION

It can be found that MnO_2 MPs display a microsphere structure with uniform diameter around 200–350 nm in field emission scanning electron microscopy (FE-SEM) images (Fig. 1a). These MnO_2 MPs are formed via the aggregation of ultrathin nanosheets with a thickness of 2–4 nm, as shown in transmission electron microscopy (TEM) images (Fig. 1b). High resolution TEM images exhibit interplanar spacing of 0.27 nm and 0.40 nm that are indexed to the (031) and (120) lattice planes of the orthorhombic γ-MnO_2 phase.[21] Selected area electron diffraction (SAED) patterns reveal four distinct diffraction rings, corresponding to the (003), (160), (131) and (031) crystal planes of orthorhombic γ-MnO_2 (inset in Fig. 1b).[24] The hybrid films have typical layered structure, and the MnO_2 MPs are dispersed and embedded in a

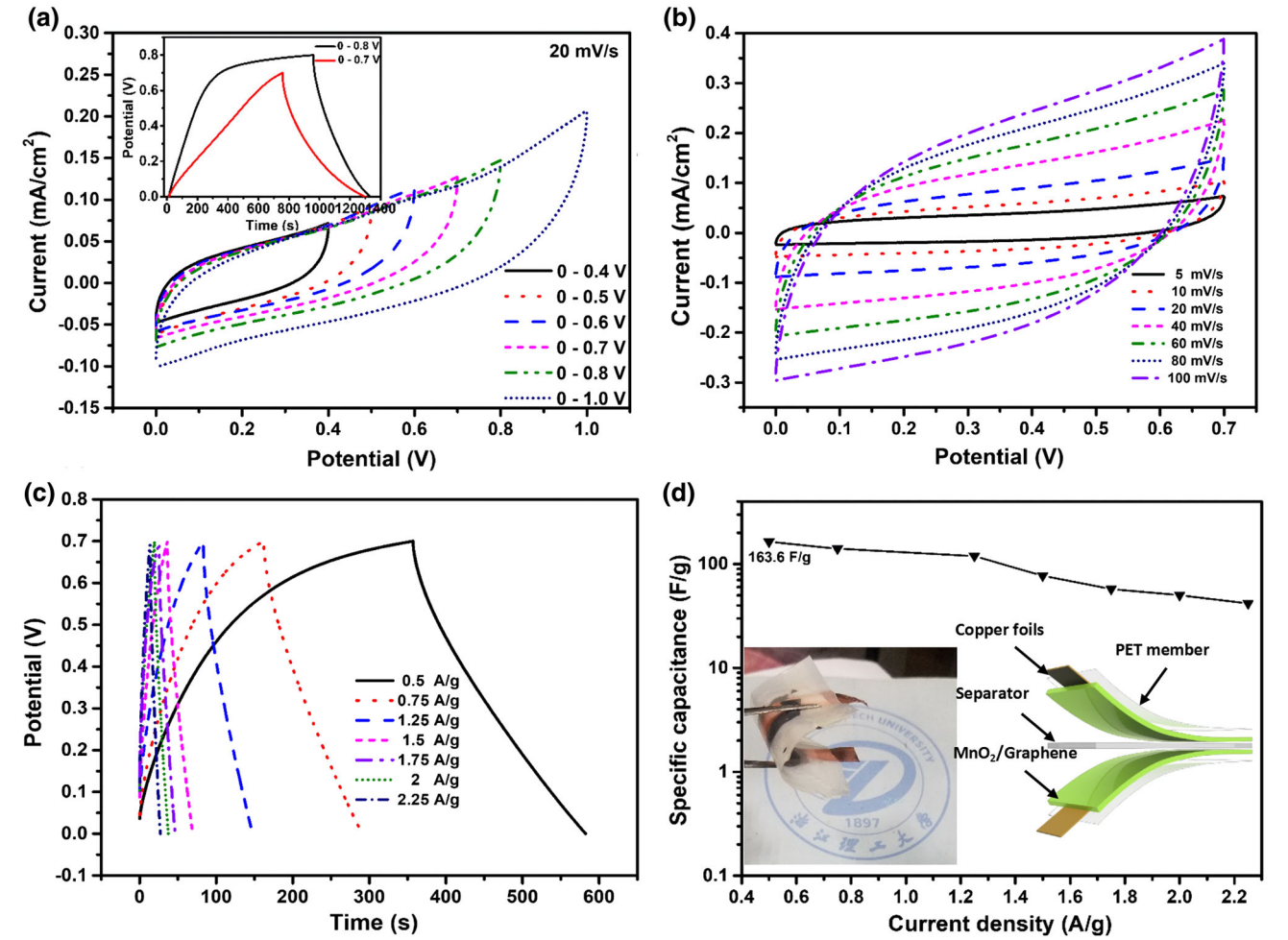

Fig. 3. (a) CV curves of MnO_2/RGO electrodes measured at different potential windows (inset shows GCD curves with a potential window at 0–0.7 V and 0–0.8 V and 0.5 A g^{-1} current density). (b) CV and (c) GCD curves of MnO_2/RGO electrodes measured under different scan rates, and (d) their specific capacitance under different current densities. The inset in (d) presents the digital picture and structure of fabricated SCs.

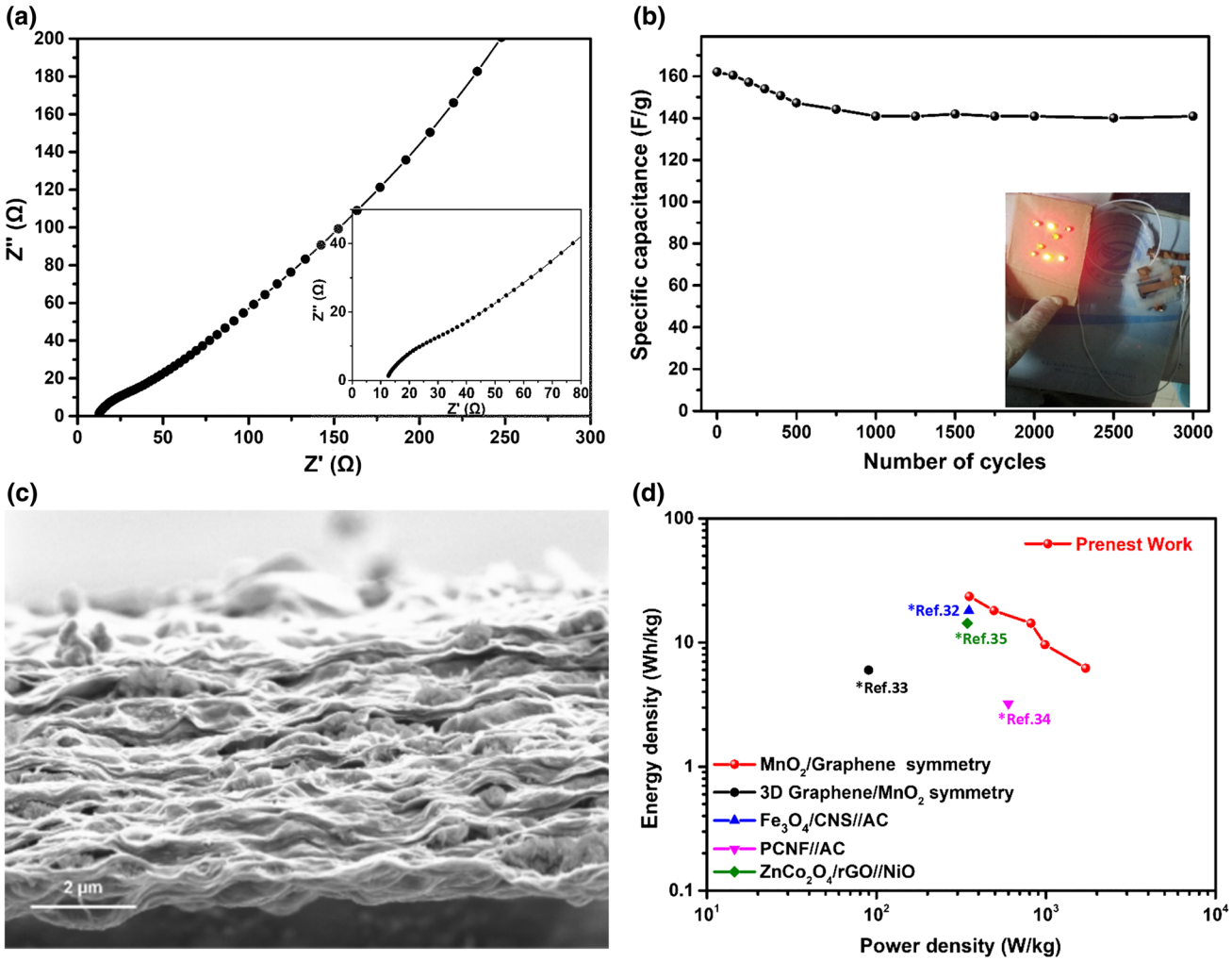

Fig. 4. (a) The EIS of fabricated SCs (inset shows the high-frequency zone). (b) Specific capacitance retention against number of cycles (inset shows the 'Z' shape LEDs lighted by fabricated SCs). (c) SEM image of MnO_2/RGO electrode after 3000 cycles. (d) Energy density versus power density variation in comparison with other SCs.

RGO layer to form hybrid films, as shown in Fig. 1c. Figure 1d shows the MnO_2/RGO hybrid films at different folding angle which indicates they possess an excellent flexible property.

The x-ray photoelectron spectra (XPS) are shown in Fig. 2a. It confirms the presence of Mn, C and O elements. The high-resolution Mn 2*p* spectrum shows the binding energy values of two main peaks at 641.8 eV (2*p*3/2) and 653.3 eV (2p1/2) (ΔE = 11.5 eV), indicating the presence a of main valence state of Mn^{4+} (Fig. 2b).[26] The weak intensity of the peaks of oxygenate bonds indicates the successful reduction of GO (Fig. 2c).[27] All the reflection peaks observed can be indexed to a tetragonal symmetry of MnO_2 with a γ-crystallographic phase from XRD patterns (Fig. 2d).[28] The lyophilized GO shows a characteristic 2θ peak at $\sim 9.5°$. In contrast, the diffraction peak in the hybrid films disappears and two wide diffractions at $\sim 13.2°$ and $25.3°$ appear, indicating the GO is reduced successfully and obtain a highly stacked structure.[29]

The hybrid films with various mass ratios of MnO_2 and GO are prepared to determine the optimal composition of electrodes. Table I shows the specific capacitance value of the electrodes with various mass ratios of MnO_2 and GO. The composition difference has no singnificant effects on the morphology and flexibility of composite films. However, the MnO_2/RGO electrodes with mass ratio of MnO_2 and GO at 10:6 exhibit the highest specific capacitance, which have been chosen as the ideal model for evaluation of the electrochemical properties of MnO_2/RGO electrodes. CV curves of the electrodes appear as a symmetric rectangular shape within an electrical window of -0.1 V to 0.7 V. Different operation voltages of SCs devices are measured to confirm the appropriate potential window in the range from 0 V to 0.7 V in 1.0 M Na_2SO_4 aqueous solution at the scan rate of 20 mV s^{-1}, as shown in Fig. 3a.[17] All of the CV curves are almost ideally rectangular with high symmetry features, indicating a good reversibility

and capacitive property of the MnO_2/RGO hybrid films (Fig. 3b).[30] The galvanotactic charge–discharge (GCD) of electrodes display nearly symmetric and linear, indicating excellent reversibility and high coulombic efficiency (Fig. 3c). The maximum specific capacitance of MnO_2/RGO electrodes is 333.9 F g^{-1} at the current density of 0.5 A g^{-1}. The maximum specific capacitance of device is 162.7 F g^{-1} at the current density of 0.5 A g^{-1}, as shown in Fig. 3d.

The electrochemical impedance spectroscopy (EIS) of the fabricated SCs displays a single small semicircle at the high frequency and a straight line with the angle of 45° at low frequency, demonstrating the low internal resistance (R_L) and excellent capacitance characteristics. Additionally, the electrical impedance (R_p) of the fabricated symmetrical SC is 10.9 Ω (Fig. 4a), illustrating good electrical conductivity.[31] The specific capacitance of the fabricated symmetrical SC retained 140.9 F g^{-1} (only 13% fading) after 3000 cycles at the current density of 0.5 A g^{-1}, indicating a high cycling stability. The morphology and structure of our MnO_2/RGO hybrid films still can be maintained after 3000 cycles (Fig. 4b). In order to study the potential application of MnO_2/RGO hybrid films, the fabricated SCs are prepared using MnO_2/RGO hybrid films as electrodes which can light the 'Z' shape LEDs (inset in Fig. 4b). After 3000 cycles, no significant change can be found on the morphology of MnO_2/RGO electrode, indicating the high stability of the electrode (Fig. 4-c). The energy density and power density of the fabricated SCs are summarized on the Ragone diagram. The obtained SCs provides a maximum energy density of 23.5 Wh kg^{-1} at 0.5 A g^{-1} (352.8 W kg^{-1} power density), which is higher than those of the other reported supercapacitors (Fig. 4d).[32–35]

CONCLUSIONS

In summary, we present a facile filtration deposition and thermal reduction method for the preparation of MnO_2/RGO hybrid films as a supercapacitor electrode material. The obtained MnO_2/RGO hybrid films possess a high specific capacitance of 333.9 F g^{-1} at the current density of 0.5 A g^{-1}. The flexible and sandwich type solid-state-symmetrical SCs based on MnO_2/RGO hybrid films have been fabricated and exhibited a safe working range with a potential window of 0–0.7 V with a maximum energy density of 23.5 Wh kg^{-1} at 0.5 A g^{-1} (352.8 W kg^{-1} power density) and the maximum power density of 1716.9 W kg^{-1} at 2.25 A g^{-1} (6.2 Wh kg^{-1} energy density). This excellent capacitance performance can be attributed to create electrolyte-accessible channels within the electrode because MnO_2 MPs are tightly anchored and sandwiched in the highly conductive graphene restacking. Such an asymmetric supercapacitor offers great promise in the application of high-performance energy storage systems because of its advantages of a low-cost, facile fabrication process, high energy and power density, and eco-friendly nature.

ACKNOWLEDGEMENTS

This work was financially supported by Collaborative Innovation Center for Modern Textile Technology of Zhejiang Province (2011-Program) (20160202) and "521 Talents Training Plan" in Zhejiang Sci-Tech University.

REFERENCES

1. H. Chen, G. Jiang, W. Yu, D. Liu, Y. Liu, L. Li, and Q. Huang, *MRS Commun.* 7, 90 (2017).
2. S. Sun, G. Jiang, Y. Liu, D. Liu, and W. Yu, *Mater. Lett.* 197, 35 (2017).
3. Y. Liu, G. Jiang, S. Sun, B. Xu, J. Zhou, Y. Zhang, and J. Yao, *J. Alloys Compd.* 731, 560 (2018).
4. Z. Tang, Z. Pei, Z. Wang, H. Li, J. Zeng, Z. Ruan, Y. Huang, M. Zhu, Q. Xue, J. Yu, and C. Zhi, *Carbon* 130, 532 (2018).
5. H. Liang, J. Lin, H. Jia, S. Chen, J. Qi, J. Cao, T. Lin, W. Fei, and J. Feng, *J. Power Sources* 378, 248 (2018).
6. Y. Tian, C. Yang, W. Que, X. Liu, X. Yin, and L. Kong, *J. Power Sources* 359, 332 (2017).
7. Y. Liu, Q. Lu, Z. Huang, S. Sun, B. Yu, U. Evariste, G. Jiang, and J. Yao, *J. Alloys Compd.* 762, 301 (2018).
8. S. Sun, G. Jiang, Y. Liu, B. Yu, and U. Evarist, *J. Energy Storage* 18, 256 (2018).
9. Y. Liu, G. Jiang, S. Sun, B. Xu, J. Zhou, Y. Zhang, and J. Yao, *J. Electroanaly. Chem.* 804, 212 (2017).
10. X. Zou, Y. Zhou, Z. Wang, S. Chen, B. Xiang, Y. Qiang, and S. Zhu, *J. Alloys Compd.* 744, 412 (2018).
11. J. Yu, F. Xie, Z. Wu, T. Huang, J. Wu, D. Yan, C. Huang, and L. Li, *Electrochim. Acta* 259, 968 (2018).
12. Y. Zhou, X. Hu, S. Guo, C. Yu, S. Zhong, and X. Liu, *Electrochim. Acta* 264, 12 (2018).
13. K. Qi, R. Hou, S. Zaman, B. Xia, and H. Duan, *J. Mater. Chem. A* 6, 3912 (2018).
14. H. Gao, F. Xiao, C.B. Ching, and H. Duan, *ACS Appl. Mater. Interfaces* 4, 7020 (2012).
15. Y. Liu, X. Miao, J. Fang, X. Zhang, S. Chen, W. Li, W. Feng, Y. Chen, W. Wang, and Y. Zhang, *ACS Appl. Mater. Interfaces* 8, 5251 (2016).
16. L. Lian, J. Yang, P. Xiong, W. Zhang, and M. Wei, *RSC Adv.* 4, 40753 (2014).
17. J. Mao, H. He, J. Qi, A. Zhang, Y. Sui, Y. He, Q. Meng, and F. Wei, *J. Electron. Mater.* 47, 512 (2018).
18. S. Lee, J. Kang, and Y. Sohn, *J. Alloys Compd.* 744, 828 (2018).
19. M. Rahmanifar, H. Hesari, A. Noori, M. Masoomi, A. Morsali, and M. Mousavi, *Electrochim. Acta* 275, 76 (2018).
20. W. Wei, X. Cui, W. Chen, and D.G. Ivey, *Chem. Soc. Rev.* 40, 1697 (2011).
21. L. Ni, Z. Wu, G. Zhao, C. Sun, C. Zhou, X. Gong, and G. Diao, *Small* 13, 1603466 (2017).
22. C. Castro, O. Crosnier, L. Athouel, R. Retoux, D. Belanger, and T. Brousse, *J. Electrochem. Soc.* 162, A5179 (2018).
23. J. Zhang, L. Dong, C. Xu, J. Hao, F. Kang, and J. Li, *J. Mater. Sci.* 52, 5788 (2017).
24. S. Devaraj and N. Munichandraiah, *J. Phys. Chem. C* 112, 4406 (2008).
25. S.N. Alam, N. Sharma, and L. Kumar, *Graphene* 6, 1 (2017).

26. L. Hu, W. Chen, X. Xie, and Y. Cui, *ACS Nano* 5, 8904 (2016).
27. W. Ma, S. Chen, S. Yang, W. Chen, Y. Cheng, Y. Guo, S. Peng, S. Ramakrishna, and M. Zhu, *J. Power Sources* 306, 481 (2016).
28. J. Yan, Z. Fan, T. Wei, Z. Qie, S. Wang, and M. Zhang, *Mater. Sci. Eng. B* 151, 174 (2008).
29. Y. Li, H. Zhang, B. Wu, and Z. Guo, *Appl. Surface Sci.* 425, 194 (2017).
30. A.V. Radhamani, K.M. Shareef, and M.S. Rao, *ACS Appl. Mater. Interfaces* 8, 30531 (2016).
31. P. Wang, C. Zhou, S. Wang, H. Kong, Y. Li, S. Li, and S. Sun, *J. Mater. Sci.* 28, 12514 (2017).
32. H. Chen, G. Jiang, W. Yu, D. Liu, Y. Liu, and L. Li, *J. Mater. Chem. A* 4, 5958 (2016).
33. H. Fan, R. Niu, J. Duan, W. Liu, and W. Shen, *ACS Appl. Mater. Interfaces* 8, 19475 (2016).
34. Y. He, W. Chen, X. Li, Z. Zhang, J. Fu, C. Zhao, and E. Xie, *ACS Nano* 7, 174 (2013).
35. Y. Liu, J. Zhou, L. Chen, P. Zhang, W. Fu, H. Zhao, Y. Ma, X. Pan, Z. Zhang, W. Han, and E. Xie, *ACS Appl. Mater. Interfaces* 7, 23515 (2015).